이학석사 학위논문

Computational Study on the Structures and Stabilities of WT α-Synuclein Protofibrils

알파시뉴클린 프로토피브릴들의 구조와 안정성에 대한 계산 연구

2021 년 8 월

서울대학교 대학원

화학부 물리화학 전공

박 윤 수

Computational Study on the Structures and Stabilities of WT α-Synuclein Protofibrils

지도 교수 신 석 민

이 논문을 이학석사 학위논문으로 제출함
2021 년 8 월

서울대학교 대학원
화학부 물리화학 전공
박 윤 수

박윤수의 이학석사 학위논문을 인준함
2021 년 8 월

위 원 장 _____

부위원장 _____

위 원 _____

ABSTRACT

Computational study on the Structures and Stabilities of WT α-Synuclein Protofibrils

Yunsu Park

Department of Chemistry

The Graduate School

Seoul National University

The intraneuronal inclusions called Lewy body is the characteristic hallmark of Parkinson's disease. The aggregated form of α-synuclein, presynaptic neuronal protein, is a major constituent of Lewy body. Recent ssNMR and cryo-EM experiments identified that wild type α-synuclein fibrils show polymorphism with two major polymorphs, called *rod* and *twister*. In particular, multiple experimental studies revealed that the α-synuclein fibrils with cytotoxicity and seeding activity adopt *rod* polymorph structures. In order to associate the cytotoxicity and seeding activity of α-synuclein fibrils

with their structural features, it is essential to explain the structural stability of the fibrils in terms of their structural features. In this thesis, we performed molecular dynamics simulations on two major polymorphs of wild type α-synuclein fibrils. Root mean square deviations, root mean square fluctuation, β-sheet contents analyses indicated that highly stable structure in aqueous environment is constructed by the cooperation of compact hydrophobic side chain core packing, backbone geometry of maximal β-sheet content wrapping the hydrophobic core structure, and the solvent exposed side chains with large fluctuations maximizing the solvation entropy. The structure of the water channel and electrostatic potential energy distribution on solvent exposed surface demonstrated how the direct interactions between water and fibril play a role in stabilizing fibril structure. We expect our study provides a basis of understanding on the pathogenic behaviors of diverse amyloid strains in terms of their structural properties.

Keywords: alpha-synuclein, polymorphism, molecular dynamics simulation, structural stability, amyloid fibril

Student Number: 2016-29784

TABLE OF CONTENTS

LIST OF FIGURES

1. INTRODUCTION

1.1. Study background

Parkinson's disease (PD), one of the most prevalent neurological disorders, affects central nervous systems of the individual[1], declining gradually patient's motor skills and cognitive functions, and there are over ten million patients with PD globally[2-3]. Despite its prevalence, the most effective and currently available treatment, Levodopa[4-5], only relieves symptoms of the disease, and does not slow or halt progression of the disease. One of the important pathological features of PD is that intraneuronal inclusions, called Lewy bodies (LB) and Lewy neurites (LN), are observed in the majority of PD patient's brain, especially *substantia nigra pars compacta* (SNc) region[1, 6]. These inclusions showed that their major constituent is an aggregated form of α-synuclein[7]. The accumulation of misfolded α-synuclein can be aggravated by duplication, triplication[8-9] or mutation of SNCA gene[10]. α-synuclein monomer can adopt two conformational states, i.e., solution (unstructured) and membrane-bound state (partially helical). Between two states, the major conformational state is its soluble form[11-12]. Despite being intrinsically disordered protein, α-synuclein monomer can adopt a series of conformations under different physiological conditions (conformational plasticity). Besides, α-synuclein monomer is known to have a tendency to

form α-synuclein fibril with cross-*β*-sheet[13-14]. Due to α-synuclein monomer's conformational plasticity and tendency to form fibril with cross-*β*-sheet, α-synuclein fibrils show various fibrillar strains[15] (polymorphism), implying that there are also various fibrillar sub-structures, i.e., oligomers and protofibrils. Various *in vitro* and *in vivo* studies suggested that the misfolding and aggregation of α-synuclein is a major pathogenic event of PD[16]. Among the various conformational states of α-synuclein aggregation, oligomers are indicated as the most potent toxic species contributing to the pathogenesis of PD[17-18]. α-synuclein oligomer varies in terms of size (dimer to multimer), type (off/on-pathway), structure and stability, indicating it has heterogeneous nature. Therefore, characterizing α-synuclein oligomers is challenging. Meanwhile, α-synuclein fibrils, once considered to be the root cause of PD, exhibit slight or no toxicity in cell culture models[19-20]. Even in certain cases of PD patients with familial mutation, there was a neuronal loss in the absence of bunch of fibrillar structures, LB[21-22]. Rather, α-synuclein fibril behaves like prion: contributing to the spread and progression of disease[23-25] like other amyloid proteins associated with neurodegenerative disorders[26-28].

Polymorphism of α-synuclein fibrils implies that fibrils can show a series of morphologies under different physiological conditions. For example, α-synuclein fibril polymorphs found in PD and multiple system atrophy (MSA) patient's brain tissue showed their different morphologies: 10nm width straight or twisted filaments hold a majority among the fibril

population, on the contrary, 5nm width straight filaments hold a minority among the fibril population[29-30]. It has been known that different α-synuclein fibril polymorphs exhibit distinct seeding: recruiting and converting native α-synuclein monomer into the fibril state[31]. Different α-synuclein fibril polymorphs also showed different toxicity *in vitro*[32] and *in vivo*[33]. Besides, brain-derived α-synuclein fibril polymorphs obtained from different synucleinopathies exhibited distinct seeding potentices in accordance with the progression rate of each disease[34]. It has been suggested that different compositions of fibril polymorphs may arise from different fibril preparations, whether obtained from patient's brain tissues or produced *in vitro*[35]. Considering that each fibril polymorph contributes distinctly to the biological activities (showing different seeding capacities and toxicities), characterizing the biological function of each fibril polymorph is essential to understand the pathological role of the fibril polymorphs. Because α-synuclein fibril polymorphs exhibit a series of morphologies, one crucially needs the molecular-level structural information like atomic resolution structure. Such structural information may give explanation on which fibril strain is major pathogenic species, which structural property contributes to the pathogenicity of fibril strain. Furthermore, it may contribute to design drugs, e.g., inhibitor, targeting α-synuclein fibrils' pathogenic local structure.

There are various experimental techniques offering structural information of α-synuclein fibrils: hydrogen/deuterium exchange nuclear magnetic resonance (HDX-NMR), electron paramagnetic resonance (EPR)

spectroscopy, micro-electron diffraction (microED), solid-state nuclear magnetic resonance (ssNMR), and cryo electron microscopy (cryo-EM)[35-41]. Among those experimental techniques, ssNMR and especially cryo-EM hold a majority of giving three dimensional structure of α-synuclein fibril at atomic resolution. Several notable findings about structural information of α-synuclein fibril have appeared: (1) 5 to 10nm width fibrils are often observed in the PD patient's brain tissue, suggesting that 5nm-width fibril might be a sub-structure of 10nm-width fibril[30, 42], (2) there are amyloidogenic segments in α-synuclein called preNAC (G47-A56) and NACore (G68-A78) region, forming tightly paired steric zippers[40]. Recently, atomic structures of α-synuclein protofibril revealed in ssNMR and cryo-EM study give more detailed structural information. In the ssNMR study[41], around 5nm-width straight single filaments structure was resolved. The structure showed its core residues were arranged in parallel, in-register β-sheets with a Greek-key topology (motifs with straight lines and right angles). The structure was stabilized by intra-protofibril interactions: (1) salt bridges (between E46-K80), (2) glutamine ladder (Q79), and hydrophobic packing of aromatic residues (F94). Meanwhile, in the cryo-EM study[35], ~10nm width straight and twisted filament structures were resolved. Unlike the ssNMR single filament structure, both cryo-EM filament structures consisted of two intertwined protofilaments, forming highly complementary steric zipper interfaces. The interfacial regions forming steric zipper were different, for the rod polymorph: preNAC (G47-A56) region and for the

twister polymorph: NACore (G68-A78) region. Both polymorphs showed a common protofilament kernel in region of H50-V77 (RMSD of 28 matched residues: 2.2 Å for Cα atoms). Interestingly, the same region (H50-V77) in the single protofilament structure revealed in the ssNMR study exhibits some similarities to the common protofilament kernel structure revealed in the cryo-EM study (RMSD of 28 matched residues: 3.4 Å for Cα atoms for two comparisons between (1) ssNMR & rod and (2) ssNMR & twister).

Although the atomic resolution structures of α-synuclein protofibril revealed in ssNMR and cryo-EM studies provide valuable structural information, both techniques have many difficulties to provide how the α-synuclein polymorph structure behaves in aqueous environment, which might be crucial to explain pathogenicity of fibril strain. But with the aid of computer simulation, one can gather such information and even more local or transient structural information which are hard to be obtained through experimental techniques.

1.2. Purpose of research

In this research, we performed molecular dynamics simulations to gain structural information of pathogenic polymorphs of wild-type α-synuclein fibrils revealed in ssNMR and cryo-EM studies. We analyzed and compared their structural features: (1) overall structural features, (2) residual level structural features, and (3) solvation properties. Those analyses were done

on the purpose of (1) trying to gain information on how the major strain obtains its structural stability in an aqueous condition which might be crucial to explain its pathogenicity, and (2) providing a basis of understanding on the pathogenic behavior of diverse amyloid strains in terms of their structural properties.

2. Methods

2.1. System setup

2.1.1. ssNMR structure

The ssNMR α-synuclein structure published by Tuttle et al. (2016) was used, which includes residues 1-140 of the peptide (PDB ID: 2N0A)[41]. Six α-synuclein fibril chains were taken from PDB and unstructured residues (1-45 and 97-140) were removed. After neutralizing terminal residues, the fibril consists of six α-synuclein chains with residues 46-96 were prepared and solvated in a dodecahedron box containing 13875 molecules of TIP3P water[43] with 43 Na^+ and 43 Cl^- counter ions to form a neutral 150 mM NaCl environment. CHARMM22/CMAP force field[44] was used for α-synuclein throughout this thesis.

2.1.2. cryo-EM rod polymorph structure

The cryo-EM structure of rod polymorph α-synuclein published by Li et al. (2018) was used, which includes residues 38-97 of the peptide (PDB ID: 6CU7)[35]. One chain was copied and located parallel to outermost chain for both of two protofilaments. Then, all terminal residues were neutralized.

The paired two protofilaments structure composed of two hexameric α-synuclein chains with residues 38-97, prepared in this way, was solvated in a dodecahedron box containing 48140 molecules of TIP3P water[43] with 145 Na^+ and 181 Cl^- counter ions to form a neutral 150 mM NaCl environment. Single protofilament system was constructed by removing the coordinates of one out of two protofilaments from the above constructed paired two protofilaments structure and solvated in a dodecahedron box containing 21529 molecules of TIP3P water[43] with 64 Na^+ and 82 Cl^- counter ions to form a neutral 150 mM NaCl environment.

2.1.3. cryo-EM twister polymorph structure

The cryo-EM structure of twister polymorph α-synuclein published by Li et al. (2018) was used, which includes residues 43-83 of the peptide (PDB ID: 6CU8)[35]. One chain was copied and located parallel to outermost chain for both protofilaments. Then, all terminal residues were neutralized. The paired protofilaments structure composed of two hexameric α-synuclein chains with residues 43-83, prepared in this way, was solvated in a dodecahedron box containing 48651 molecules of TIP3P water[43] with 141 Na^+ and 153 Cl^- counter ions to form a neutral 150 mM NaCl environment. Single protofilament system was constructed by removing the coordinates of one out of two protofilaments from the above constructed paired two protofilaments structure and solvated in a dodecahedron box containing

21262 molecules of TIP3P water[43] with 62 Na^+ and 68 Cl^- counter ions to form a neutral 150 mM NaCl environment.

2.2. Simulation protocols

First, all prepared systems were minimized by steepest descent algorithm (10000 steps) and conjugated gradient algorithm (10000 steps), sequentially. After minimization, systems were gradually heated for 6.2 ns from 0 K to 310 K with position restraints on backbone heavy atoms (force constant k = 100 kJ/mol/nm^2). For pre-equilibration, several 2 ns runs were performed at 310 K with restraints of decreasing orders of strength (k = 100, 50, 30, 10 kJ/mol/nm^2). Each system was further equilibrated at 310 K for 10 ns without position restraints to obtain the initial conformations for the product run. For all heating and equilibration steps throughout this thesis, the isothermal–isobaric ensemble (NPT ensemble) with a velocity-rescaling thermostat[45] and a Berendsen barostat[46] was used. After equilibration, product runs were performed (1 μs for ssNMR structure and two single protofilament cryo-EM structures, and 500 ns for two paired protofilament cryo-EM structures). Trajectories were saved every 2 ps for analysis. All product runs were performed using the NPT ensemble with a velocity-rescaling thermostat[45] and a Parrinello-Rahman barostat[47], and a 2 fs time step was used with the LINCS algorithm[48] for the constraints of bonds related with hydrogen atoms. GROMACS 2020.4 package[49] was used for all

simulations.

2.3. Analysis

β-sheet contents were calculated by DSSP algorithm[50-51] in GROMACS[49]. Electrostatic potential maps of each structure at the solvent accessible surface were calculated by solving the nonlinear Poisson-Boltzmann equation using APBS Electrostatics plugin[52] in PyMOL[53]. Single Debye-Hückel boundary condition, cubic B-spline discretization of point charges on grid, and smoothed surface were used for dielectric and ion-accessibility coefficients at 310 K. Dielectric constants $\varepsilon_{protein}$=2.0 and ε_{water}=78.0 were used and ion concentrations were 150 mM for Na^+ (radius=1.02 Å) and Cl^- (radius=1.81 Å).

3. Overall structural features

3.1. Introduction

Tuttle et al identified a high-resolution structure of wild type α-synuclein with single protofilament Greek-key *β*-sheet topology by ssNMR and X-ray spectroscopies[41]. They added the fibrils to primary hippocampal neurons and observed the induction of insoluble inclusions. They also showed that the same α-synuclein fibrils act as pathological seeds which initiate a disease. Although the ssNMR structure of the fibril has a single protofilament morphology, it is possible that the fibril presents in the form of a pair of two protofilaments when it is inside the neuronal cells. Li et al showed that the *in vitro* generated α-synuclein fibrils demonstrated a dose-dependent cytotoxicity and seeding activity[35]. By cryo-EM study, they found that two major populations, referred to as “rod” and “twister” consist of the fibrils. The rod polymorph also has Greek-key *β*-sheet topology which is very similar to the ssNMR structure identified by Tuttle et al. However, the rod polymorph consists of a pair of two tightly mated protofilaments. Therefore, we may postulate that the rod protofilament with Greek-key *β*-sheet topology is a major pathogenic strain. In order to verify it in terms of the structural stabilities, we performed the simulations on the above experimental structures (ssNMR, cryo-EM rod, cryo-EM twister) and

compared the structural features.

3.2. Results and discussion

3.2.1. Single protofilament rod-like structures simulation

At first, we performed simulations using two different initial structures having Greek-key β-sheet topology. One is from ssNMR structure by Tuttle et al[41] and the other is from cryo-EM structure by Li et al[35], which are denoted as "rod_{ssNMR}" and "$rod_{cryo\text{-}EM}$" respectively in **Figure 3.4.1**. When compared with paired structures, we will denote the single protofilament rod polymorph as "rod_{single}" instead of "$rod_{cryo\text{-}EM}$". **Figure 3.4.1** shows the two structures before simulations and after 1μs simulations (left) and the changes of root mean square distance (RMSD) values during the simulations (right). After 1μs simulations in aqueous environment, the two converged structures show both common and different features. Both of the two structures adopt compact interior side chain packing with steric zipper geometries. In contrast, the side chains at solvent exposed surfaces adopt a more disordered arrangement compared to initial configurations in order to maximize the solvent accessible surface area. In consequence, the optimal backbone geometry in aqueous environment is formed in compliance with these two - hydrophobic and hydrophilic side chain rearrangements for the purpose of achieving a maximal structural stability through the most

preferable interactions with water. In other words, various structural features of the α-synuclein fibril can be interpreted in the aspect of stabilizing structures via interaction with water. Therefore, the differences in structural features as well as common features between different geometry of fibrils and their relative stabilities in aqueous condition, which might be a crucial factor of the pathogenicity and seeding activity of specific fibril strains, can also be explained in the same way. Rod_{ssNMR} structure decreases its β-sheet content after simulation as can be seen in **Figure 3.4.1**, while $rod_{cryo\text{-}EM}$ structure shows slightly increased area of backbone having β-sheet content. Another difference is, $rod_{cryo\text{-}EM}$ structure shows significant increase of disordered arrangement of C-terminal and N-terminal residues after simulation, while rod_{ssNMR} structure maintains ordered arrangement of terminal residues. These distinct differences between two apparently highly similar structures demonstrate that the interactions between water or other solvents and fibril delicately control the fibril conformation in order to achieve maximal structural stability. It can be summarized that rod_{ssNMR} structure is not preferred in aqueous environment because its side chain arrangement and corresponding backbone geometry is adapted to dry conditions while $rod_{cryo\text{-}EM}$ structure is optimized for aqueous condition and will gain high structural stability in aqueous environment. It can be predicted that rod_{ssNMR} structure will pass through the conformational change in $rod_{cryo\text{-}EM}$ structure when it is placed in aqueous environment.

In the paper of Tuttle et al[41], the disordered region and the core region are defined as residues 55 to 62 and residues 46 to 54, 63 to 96 respectively. RMSD curves in **Figure 3.4.1** show that disordered region of rod_{ssNMR} structure is actually disordered while the same region in $rod_{cryo\text{-}EM}$ structure relatively low fluctuation due to the formation of well ordered β-sheet geometry. The comparison of RMSD curves shows that even the fluctuations of the core region is relatively small in $rod_{cryo\text{-}EM}$ structure, which is due to both well arranged β-sheet backbone structure and highly compact sidechain packing structure of hydrophobic core kernel. On the other hand, the fluctuations of backbone and inside side chains are very small while the outside side chains show large fluctuations. In particular, for cryo-EM structure, the fluctuation of inside side chains is even smaller than the backbone while the fluctuations of outside side chains are large. Along with static structural features explained above, these dynamic features show that $rod_{cryo\text{-}EM}$ fibril has highly stable structure in aqueous environment constructed by the cooperation of compact hydrophobic side chain core packing, backbone geometry of maximal β-sheet content wrapping the hydrophobic core structure, and the solvent exposed side chains with large fluctuations maximizing the solvation entropy. By comparing with rod_{ssNMR} structure, these features have been more clearly revealed.

3.2.2. Paired rod-like structure

Figure 3.4.2 shows the simulation results of rod polymorph consisting of two interfaced $rod_{cryo\text{-}EM}$ protofilaments which we denote "rod_{pair}" for convenience in this thesis. The most notable change in RMSD curves of rod_{pair} structure compared to rod_{single} ($rod_{cryo\text{-}EM}$ in **Figure 3.4.1**) is that the fluctuation of the disordered region (defined as residues 55-62 in ssNMR structure) is reduced while the core region fluctuation is increased. This change is due to the formation of the interface between two protofilaments. Examining the superimposed structures in **Figure 3.4.2** shows that the backbone geometry becomes flat as it forms an interface, of which the conformational change propagates to adjacent sequences and derives the overall slight rearrangement of backbone geometry. In consequence, paired structure provides additional stability especially at the interface region by forming steric zipper interaction and hiding the hydrophobic residues at the interface from exposure to water. This stable interface structure allows slight increase of fluctuation in the rest part of the structure which can give additional conformational and solvation entropy.

3.2.3. Twister structure and fluctuation features

Figure 3.4.3 shows the simulation results of twister polymorphs which will be denoted by "$twister_{single}$" and "$twister_{pair}$" for single protofilament structure (**Figure 3.4.3. a, b**) and the structure consists of pair of two protofilaments (**Figure 3.4.3. c**), respectively. Twister polymorph has less

compact backbone geometry than the rod polymorph with highly compact Greek-key β-sheet geometry. Therefore, it has a more flexible and less stable backbone β-sheet structure and hydrophobic core structure. In addition, the twister polymorph has a different interface structure with rod polymorph. The rod polymorph has preNAC ($_{47}$GVVHGVATVA$_{56}$) interface, while twister has NACore ($_{68}$GAVVTGVTAVA$_{78}$) interface. Although both of them form steric zippers and NACore sequence is included in highly hydrophobic NAC (61-95) region, a linear backbone geometry and the orientations of bulky hydrophobic side chains with salt bridge interactions between E57 and H50 allow the preNAC sequence to form cross β-sheet interface structure of rod polymorph, which is more rigid and stable than the bent shape NACore interface of twister polymorph.

Due to these differences in interface structures along with side chain interactions in hydrophobic core regions, twister polymorph (**Figure 3.4.3. a**) is relatively unstable and more flexible in aqueous environment. In particular, the compactness of the hydrophobic core and backbone structure is not enough to handle the instability of the hydrophobic interface region. As a result, the backbone β-sheet planes, especially around the interface region, are twisted along the fibril axis in order to adopt a more stable geometry in aqueous environment - increase of hydrophilic surface and more compact hydrophobic core side chain packing (**Figure 3.4.3. b**). As the twister polymorph consisting of a pair of two protofilaments form hydrophobic steric zipper interface which fixes the problem of single

protofilament and stabilizes the structure, the extent of backbone helical rotation is apparently reduced. This modest amount of rotation would be essential to form helical structure of twister polymorph because too short pitch distance will not be compatible with the persistent length of backbone *β*-sheet structure. In fact, single protofilament twister structure is not experimentally observed, of which the reason could be explained through this interpretation.

3.2.4. Backbone *β*-sheet structure analysis

In order to compare the geometries of backbone structures in our simulations, the secondary structure contents were calculated using the DSSP algorithm. In particular, the backbone *β*-sheet contents and the structural patterns are shown in **Figure 3.4.4** and **Figure 3.4.5**. As can be seen in the secondary structure pattern (**Figure 3.4.5**), all five structures mostly consist of *β*-sheet and turn. In particular, rod_{pair} shows distinct placement of turns (yellow color) between *β*-sheets (red color) compared to the other structures (**Figure 3.4.5**). **Figure 3.4.4. (a)** (*β*-sheet content per single α-synuclein chain) shows the following trends: (1) *β*-sheet contents of twister polymorph > *β*-sheet contents of rod polymorph. That is, the less compact backbone structure is advantageous for large *β*-sheet content. It implies that large *β*-sheet content does not guarantee the stability of fibril structure. Although *β*-sheet backbone is generally preferred in aqueous

environment in order to form hydrophobic side chain core, solvent exposed surface of hydrophilic side chains, and β-sheet hydrogen bonding, the flexible β-turn-β motif rather than more linear β-sheet motif (see **Figure 3.4.4. b**) could more effectively make highly compact folding structure of hydrophobic core. In addition, the relatively short length of β-sheet stretches consisting of β-turn-β geometry compared to more linear and less compact backbone geometry, is beneficial in forming stable backbone β-sheet hydrogen bonding interactions. (2) For both rod and twister polymorphs, β-sheet contents of single protofilament structures > β-sheet contents of paired protofilament structures. The formation of an inter-protofilament interface protects the hydrophobic residues exposed to water by exploiting them to use in hydrophobic steric zipper structure. The decrease of β-sheet contents for paired structure compared to single protofilament structure is a consequence of this process. (3) β-sheet contents of ssNMR structure is the least. It simply reflects that this structure is relatively inadequate in aqueous environment.

3.3. Conclusion

In previous paragraphs, we have analyzed the overall static and dynamic (i.e. fluctuation) features of experimentally identified α-synuclein protofibril structures by careful examination of β-sheet contents and RMSD curves.

3.4. Figures

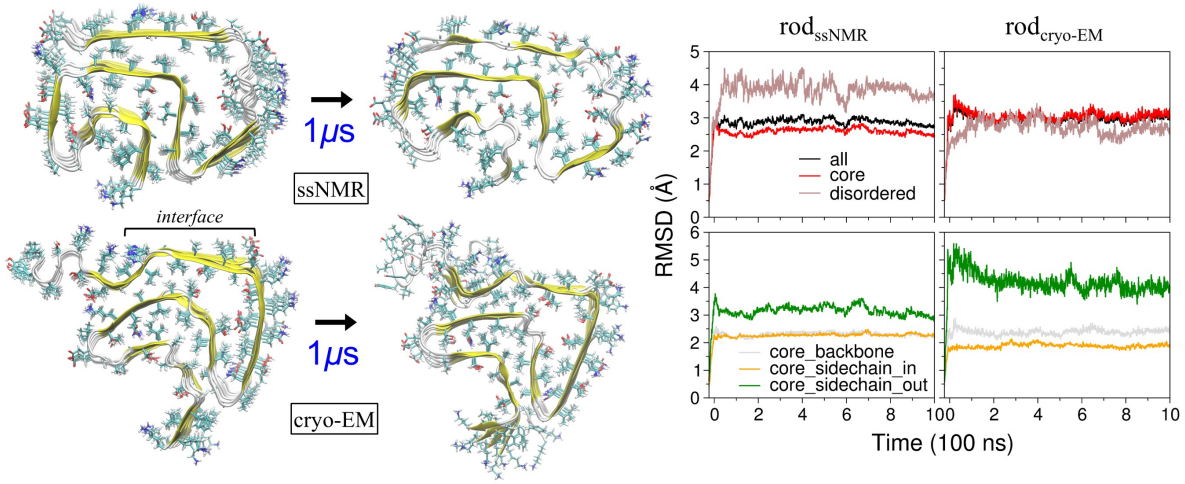

Figure 3.4.1.

(*left*) Experimental rod structures of α-synuclein protofilament from ssNMR and cryo-EM experiments, and their converged structures after 1μs simulations in aqueous environment. (*right*) RMSD curves from the simulations. RMSD curves for whole sequence (residues 46-96), core region (residues 46-54, 63-96), disordered region (residues 55-62) are shown in black, red, and brown colors, respectively where core and disordered regions are defined from ssNMR data[41]. For core region, RMSD curves for backbone (grey), side chains buried inside (orange), and side chains exposed outward (green) are separately plotted.

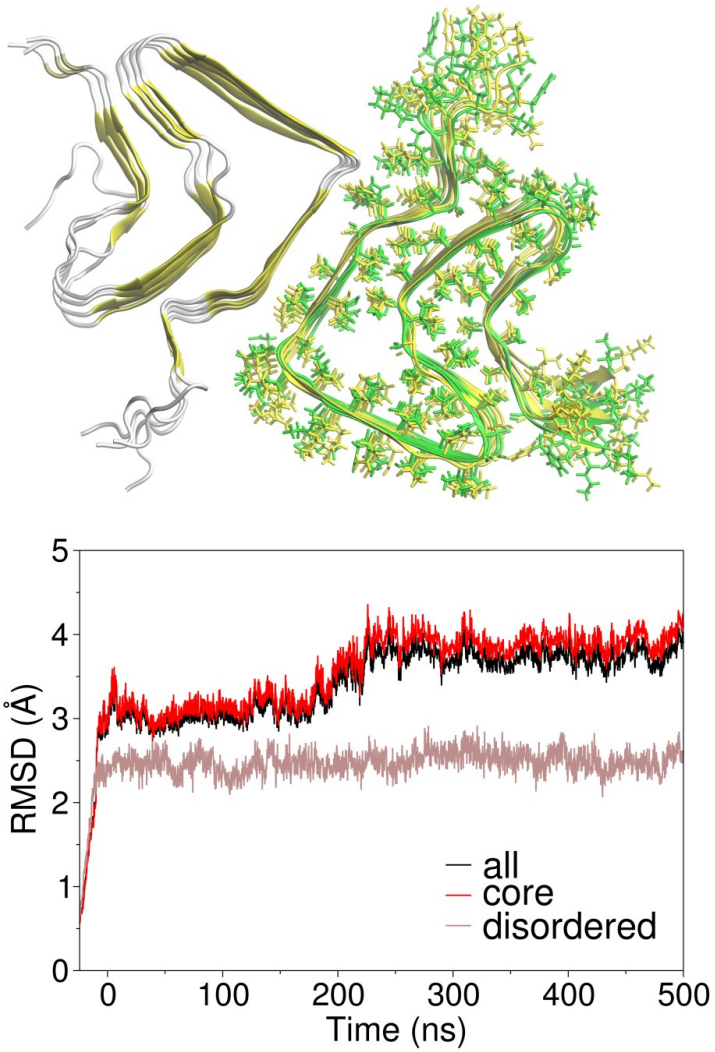

Figure 3.4.2.

Paired two protofilaments rod structure after 500ns simulation (yellow) and corresponding RMSD curves. For comparison, a simulation structure of single protofilament (green) is superimposed.

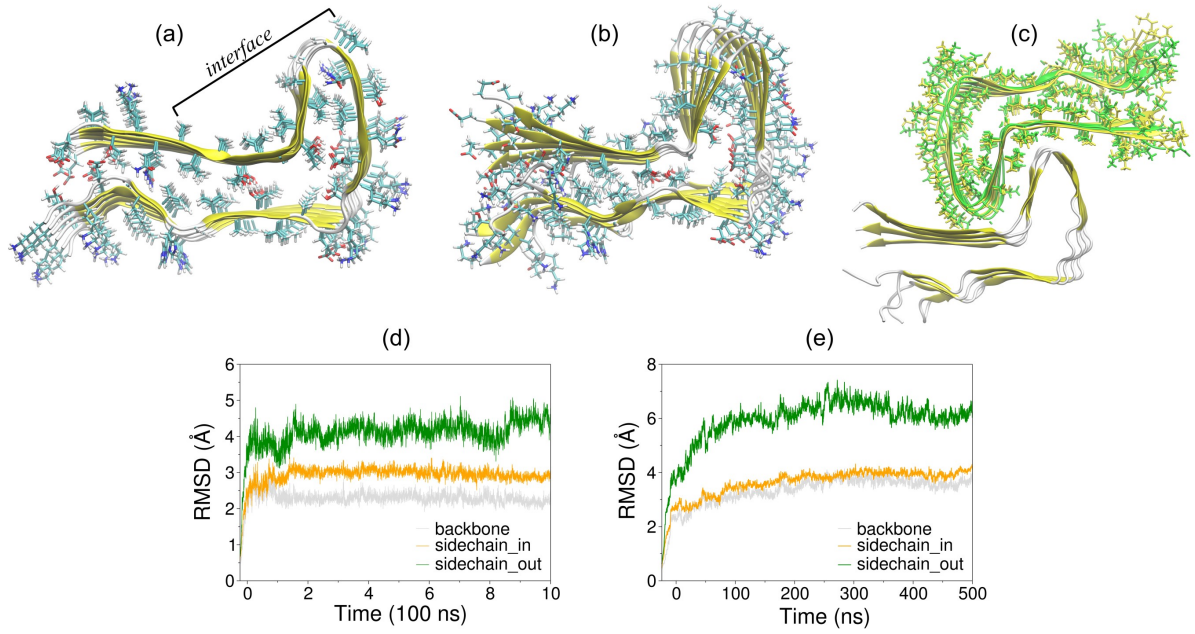

Figure 3.4.3.

Simulation results of twister structures. (a) Experimental cryo-EM structure (b) Structure after 1μs simulation (c) Paired two protofilaments structure after 500ns simulation (yellow), on which a single protofilament simulation structure (green) is superimposed for comparison (d) RMSD curves from 1μs simulation of a single protofilament structure (e) RMSD curves from 500ns simulation of paired two protofilaments structure. RMSD curves for backbone (grey), side chains buried inside (orange), and side chains exposed outward(green) are separately plotted.

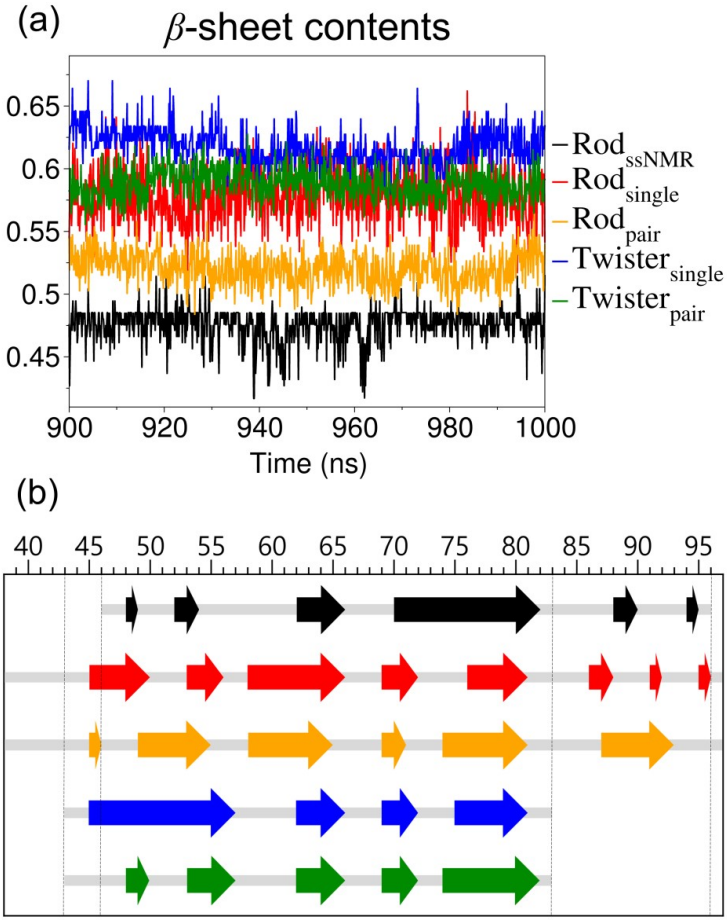

Figure 3.4.4.

(a) β-sheet contents during the last 100ns of each simulation for ssNMR rod structure (Rod_{ssNMR}), single protofilament rod structure (Rod_{single}), paired two protofilaments rod structure (Rod_{pair}), single protofilament twister structure ($Twister_{single}$), and paired two protofilaments twister structure ($Twister_{pair}$) (b) Backbone β-sheet geometries of five structures obtained from (a).

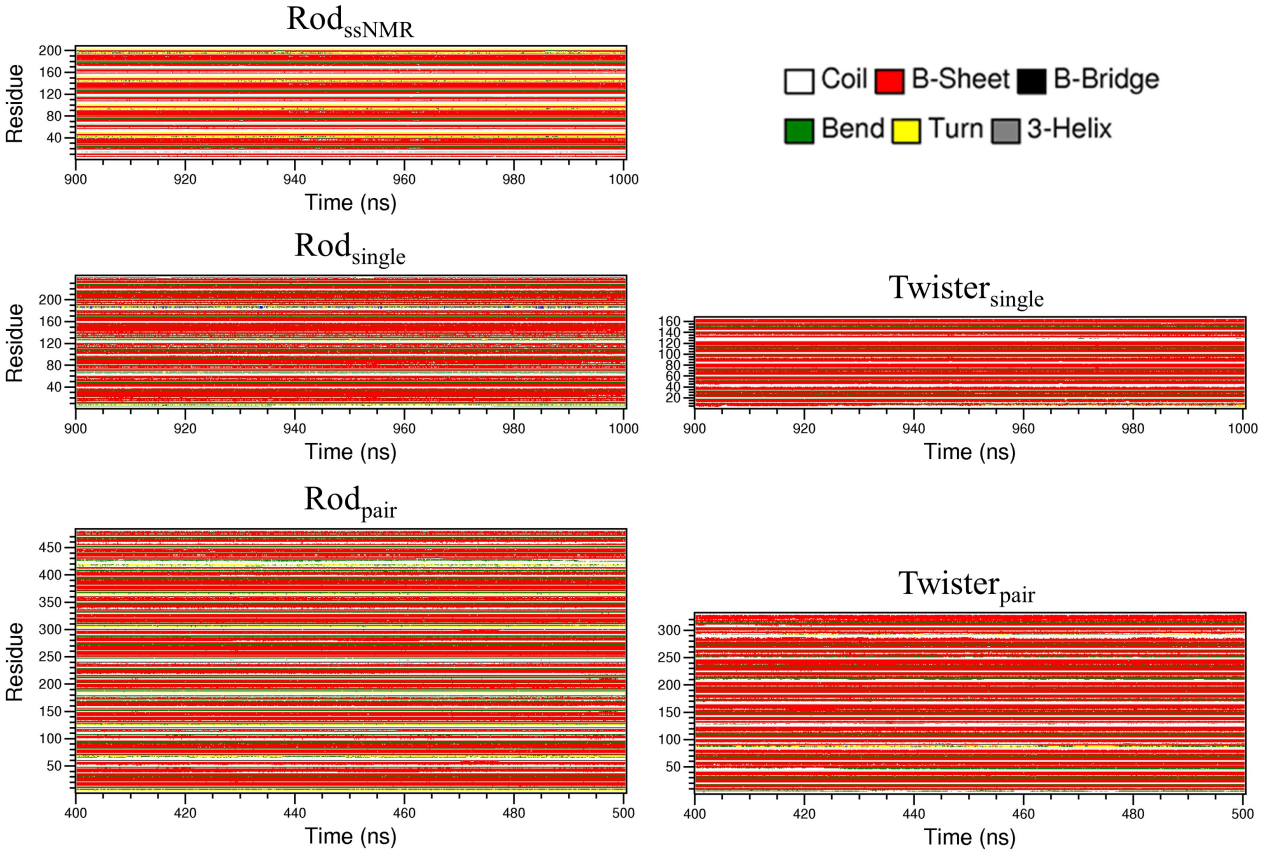

Figure 3.4.5.

Secondary structure maps calculated by DSSP algorithm for the last 100ns of each trajectory of five different structures.

4. Residue level structural features

4.1. Introduction

In order to gain more detailed structural information, we have done amino acid residue level investigation on (1) the conformational and fluctuation features for all simulated structures by calculating and analyzing the root mean square fluctuations (RMSFs) and (2) the structures of the water channels of three different fibril polymorphs.

4.2. Results and discussion

4.2.1. Comparison of overall RMSF plot shape features

In **Figure 4.4.1**, the backbone (C_α) RMSF graphs show alternated peak-and-valley pattern in which the peaks and valleys correspond to turns and β-sheet sequence, respectively. The locations of the peaks are denoted by thick bars labeled by letters a, b, c, etc. For example, b, c, d, and e in rod polymorphs and b, c, and d in twister polymorphs are the locations of the turns. The large peaks of side chain RMSF graphs occur at turn geometries (b and e of rod polymorphs and b and c of twister polymorphs) because of bulky side chains exposed to solvent. The low side chain RMSF regions

(valleys) correspond to side chains participating in the hydrophobic core packing or inter protofilament interface structures.

Figure 4.4.2 shows the structures of these regions in detail. By comparing these structures and the corresponding RMSF values, the structural features at residue level can be associated with accompanied fluctuations which cooperatively contribute to the overall structural stabilities of the corresponding polymorphs. For example, in rod polymorph, a is at the interface region and the RMSF values at a are rod_{single} > rod_{pair}. b has bulky E-K-K-Q solvent exposed residues which is reflected in the large peak of the side chain RMSF graph. Small RMSF peak of rod_{pair} at c indicates a slight rearrangement backbone due to interface formation. In twister polymorph, a is located near the N-terminal and shows large RMSF values. b and c are turns and the solvent exposed bulky side chains produce large RMSF values. Low RMSF of rod_{pair} at d is because of adjacent position to interface structure.

4.2.2. Water coordination structures

In **Figure 4.4.3**, we showed the structures of the water channels of three different fibril polymorphs. The rod_{ssNMR} polymorph has a water channel consisting of three polar amino acid residues that form hydrogen bonding with water molecules (E61, T59, and T72). This relatively small water channel allows only first and second hydration shells and isolated water

molecules, which are shown in **Figure 4.4.3 (a)**. Similarly, a twister polymorph also has first and second hydration shells, but with narrower space (only two residues, E61 and T72 participate in hydrogen bonding with water) which is indicated by lower peaks of radial distribution functions in **Figure 4.4.3 (d)**. On the other hand, the $rod_{cryo\text{-}EM}$ polymorph has a water channel of relatively large space consisting of four hydrogen-bonding participating residues (E61, T59, T54, and T75) which allows the third hydration shell shown in **Figure 4.4.3 (d)** as broad RDF peak at > 5.5Å.

4.2.3. Possible effects on structural stability

This hydrogen bonding network of the water channel can operate as an additional structural stability factor by coordination with internal side chains which would be otherwise apart from each other. Concomitantly, the hydrogen bonding network in the water channel allows the conformational flexibility to the structure of associated backbone sequence, which is participating in the formation of steric zipper fibril interface, which in consequence makes the overall structure more stable.

4.3. Conclusion

So far, we have seen that the aqueous environment drives the fibril to adopt the highly stable structure from overall hydrophobic core - hydrophilic

surface construction to the residue level conformational arrangement with associated fluctuation patterns. Meanwhile, solvent waters also can affect the stability of fibril structure by direct interactions: the coordination of water molecules with polar amino acid residue side chains in the water channel.

4.4. Figures

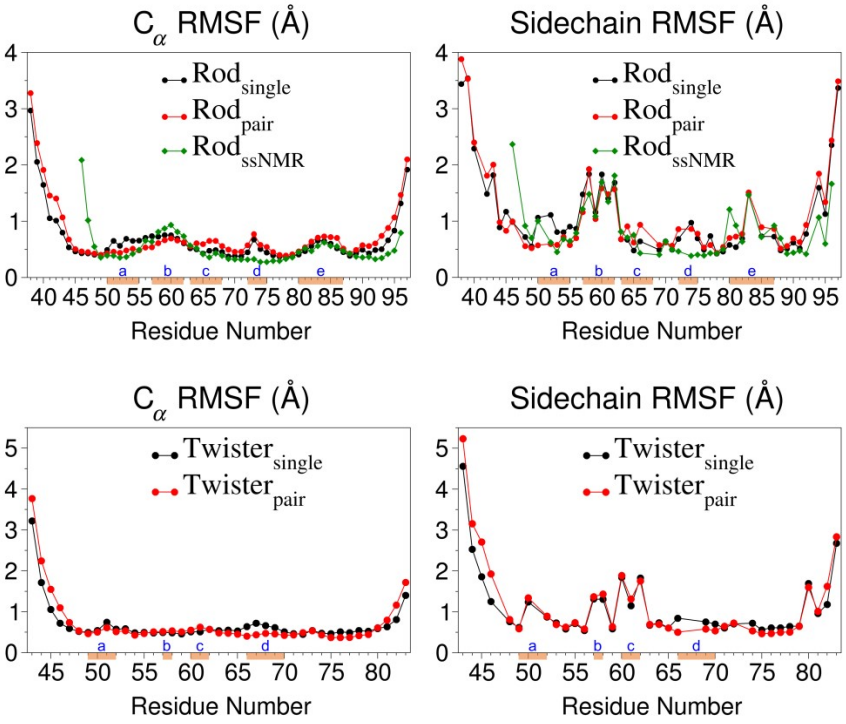

Figure 4.4.1.

Root mean square fluctuations (RMSF) of C_α (left column) and sidechain (right column) for each residue of rod polymorphs (top row) and twister polymorphs (bottom row). The thick brown bars with the letters a, b, c … upon them denote the characteristic positions - mainly the peaks, where corresponding structures are shown in **Figure 4.4.2**.

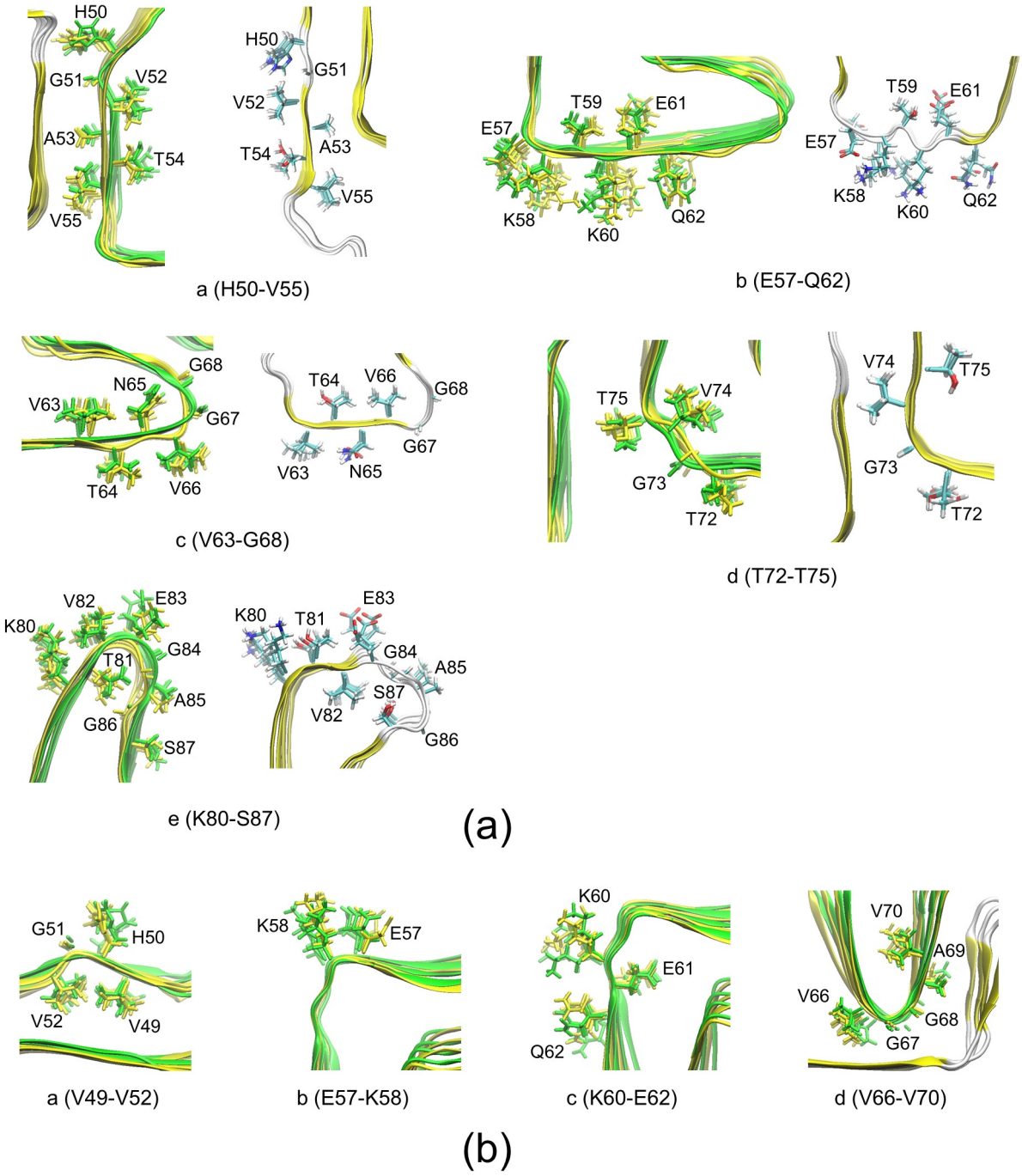

Figure 4.4.2.

(The caption of the above figure is on the next page)

(a) Structures of sequences denoted by a, b, c, d, e in RMSF graphs of **rod** polymorphs in **Figure 4.4.1**. Shown the on left side, single protofilament structure (Rod_{single}, green) is superimposed on paired two protofilament structure (Rod_{pair}, yellow) for comparison. On the right side, Rod_{ssNMR} structure is drawn in yellow backbone and colored side chains (b) Structures of sequences denoted by a, b, c, d in RMSF graphs of twister polymorphs in **Figure 4.4.1**. Single protofilament structure ($Twister_{single}$, green) is superimposed on paired two protofilament structure ($Twister_{pair}$, yellow) for comparison.

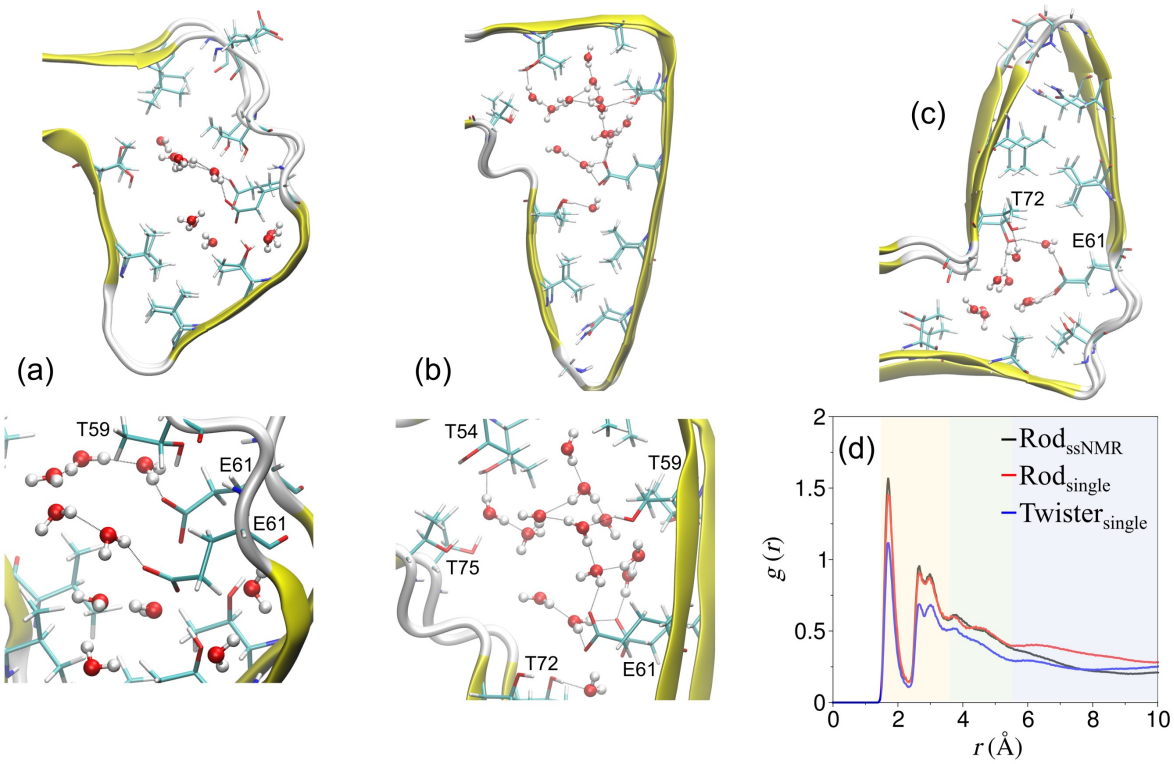

Figure 4.4.3.

The structures of water channels in the simulations of (a) ssNMR structure (b) cryo-EM rod structure (c) cryo-EM twister structure, and (d) radial distribution functions of water around residue E61. Yellow, green, and blue background colors denote the areas of different hydration shells.

5. Solvation properties

5.1. Introduction

The other direct interaction of solvent water is the interactions with the solvent exposed surfaces of fibril polymorphs. Electrostatic potential maps on the solvent exposed surfaces of fibril polymorph structures and radial distribution functions of water around the residues on fibril surface were calculated to give explanation on the interactions of fibril polymorphs with solvent water.

5.2. Results and discussion

5.2.1. Electrostatic potential energy surface structures

Figure 5.4.1 shows the electrostatic potential energy maps on these solvent exposed surfaces. According to these maps, the surfaces are composed of water channels, unstable (high energy) surfaces, and stable (low energy) surfaces. Despite various conformational features providing high structural stability as we have described above, the solvent accessible surface at N-terminal sequence which is adjacent to interface sequence, shows high electrostatic potential energy values in rod_{single} polymorph, which is even

more unstable than ssNMR structure. Therefore, the rod polymorph of paired state would be preferred in order to conceal this surface from water (**Figure 5.4.2**). On the other hand, the large solvent exposed pocket at C-terminal sequence is stabilized by hydrogen bonding between solvent water and S87 residue (see RDF in **Figure 5.4.3**). In a twister polymorph, the hydrophobic surface at the interface region can be stabilized by forming the paired polymorph (see **Figure 5.4.1** and **Figure 5.4.4**).

5.2.2. Solvation structures and water channel

The water radial distribution functions of V74 and V66 indicate that this region highly disfavors the interaction with waters (**Figure 5.4.5**). The water channel of rod_{ssNMR} polymorph has a narrow ellipsoidal shape while $rod_{cryo\text{-}EM}$ has a round shape channel allowing more water molecules inside.

5.3. Conclusion

From the electrostatic potential maps at the solvent accessible surface from the simulation of fibril polymorph structure, it can be suggested that single protofilament structures of rod and twister would prefer their paired state in order to conceal the unstable surfaces. And solvation structures of fibril polymorphs can be explained with the aid of water RDFs of exposed pocket and interfacial residues.

5.4. Figures

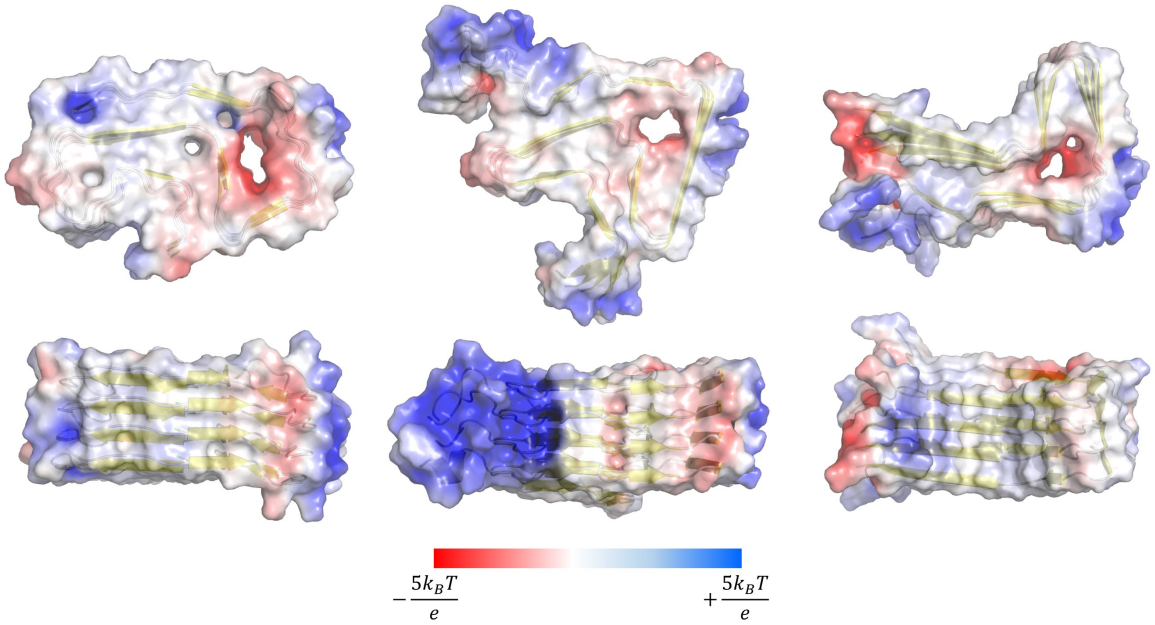

Figure 5.4.1.

Electrostatic potential maps at solvent accessible surfaces of the structures in aqueous environment derived from the simulations of ssNMR (left), cryo-EM rod (middle), and cryo-EM twister (right).

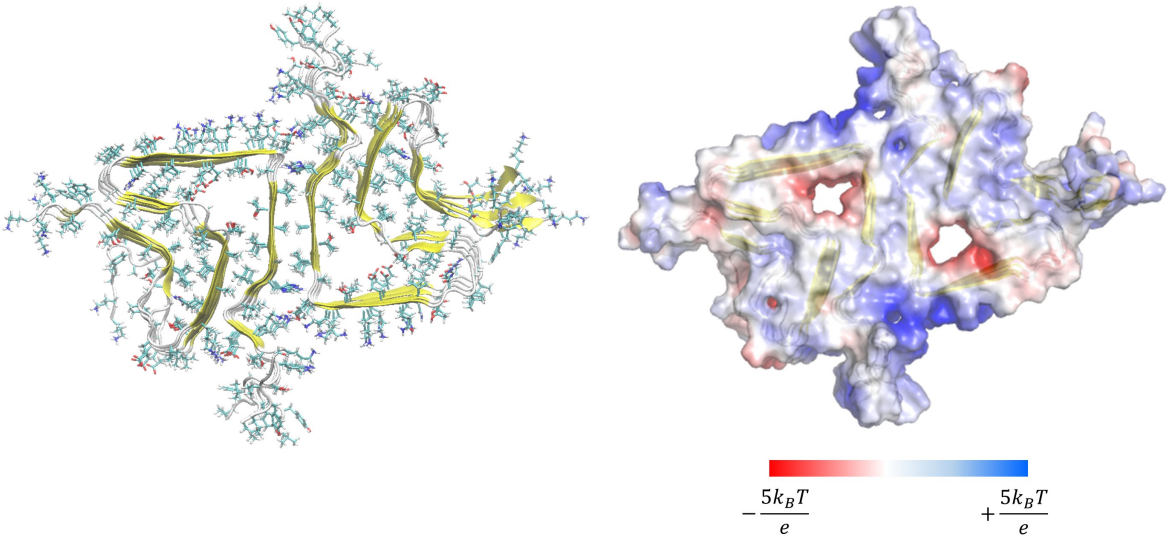

Figure 5.4.2.

Electrostatic potential map at the solvent accessible surface from the simulation of rod polymorph with a pair of two interfaced protofilaments

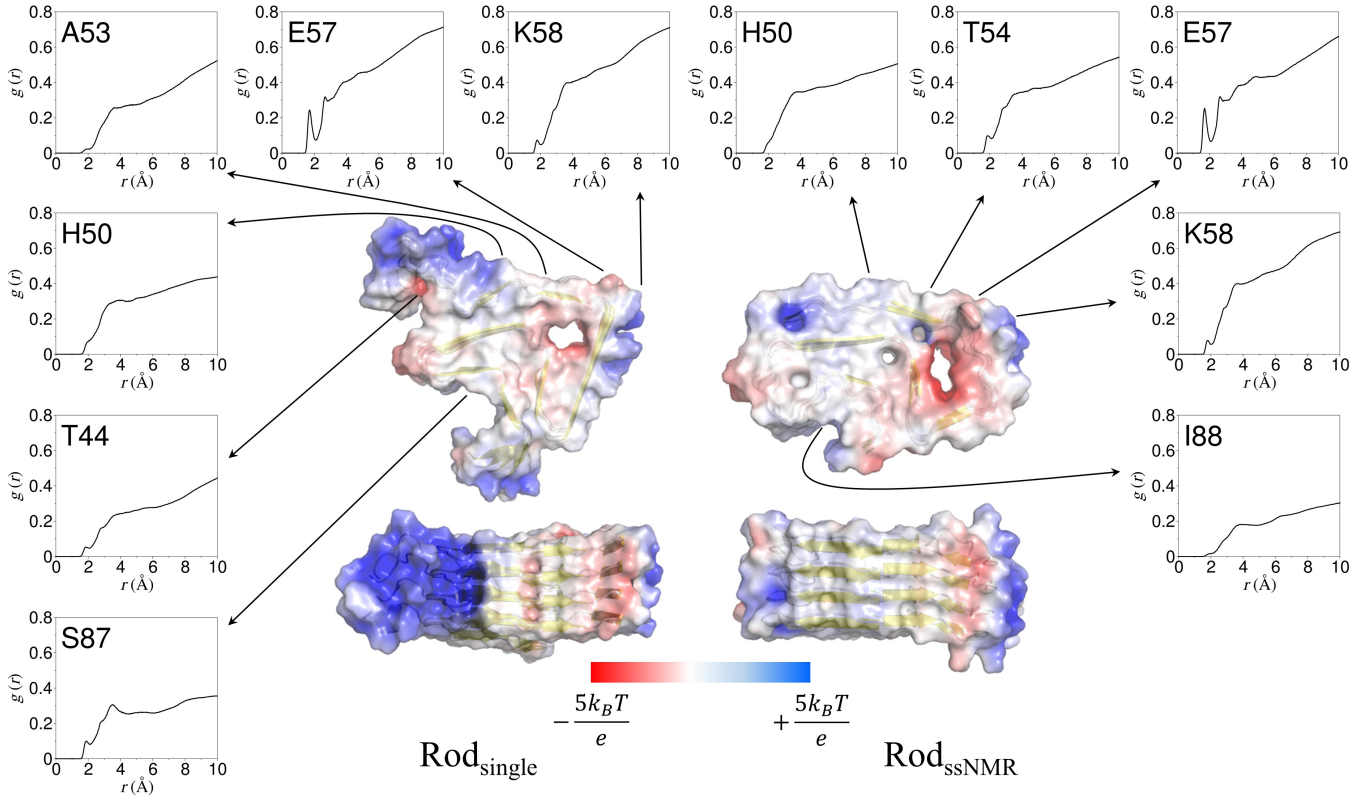

Figure 5.4.3.

Electrostatic potential maps at the solvent accessible surface from the simulations of single rod protofilament structures (left: cryo-EM, right: ssNMR), with radial distribution functions of water around the residues at interface region (Rod$_{single}$: H50, A53, E57, K58 / Rod$_{ssNMR}$: H50, T54, E57, K58) and the residues at the pocket shape surfaces (Rod$_{single}$: T44, S87 / Rod$_{ssNMR}$: I88)

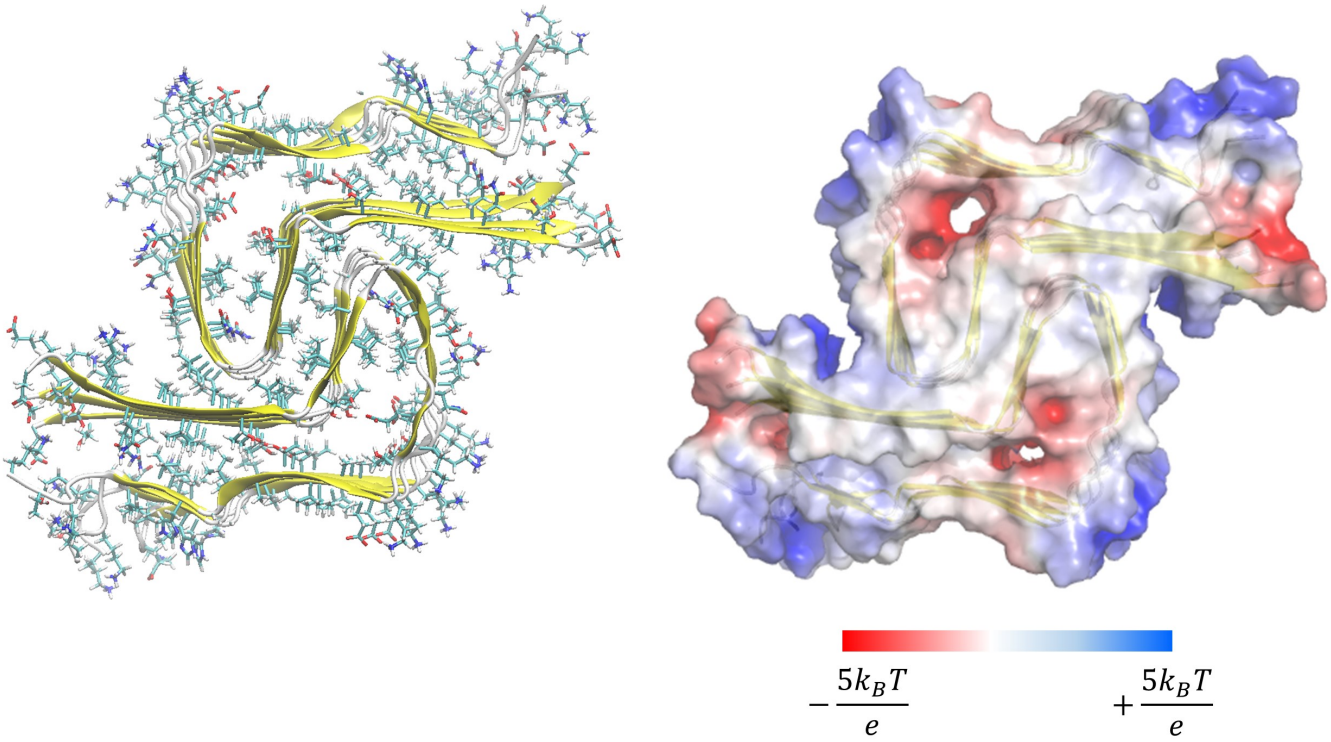

Figure 5.4.4.

Electrostatic potential map at the solvent accessible surface from the simulation of twister polymorph with a pair of two interfaced protofilaments

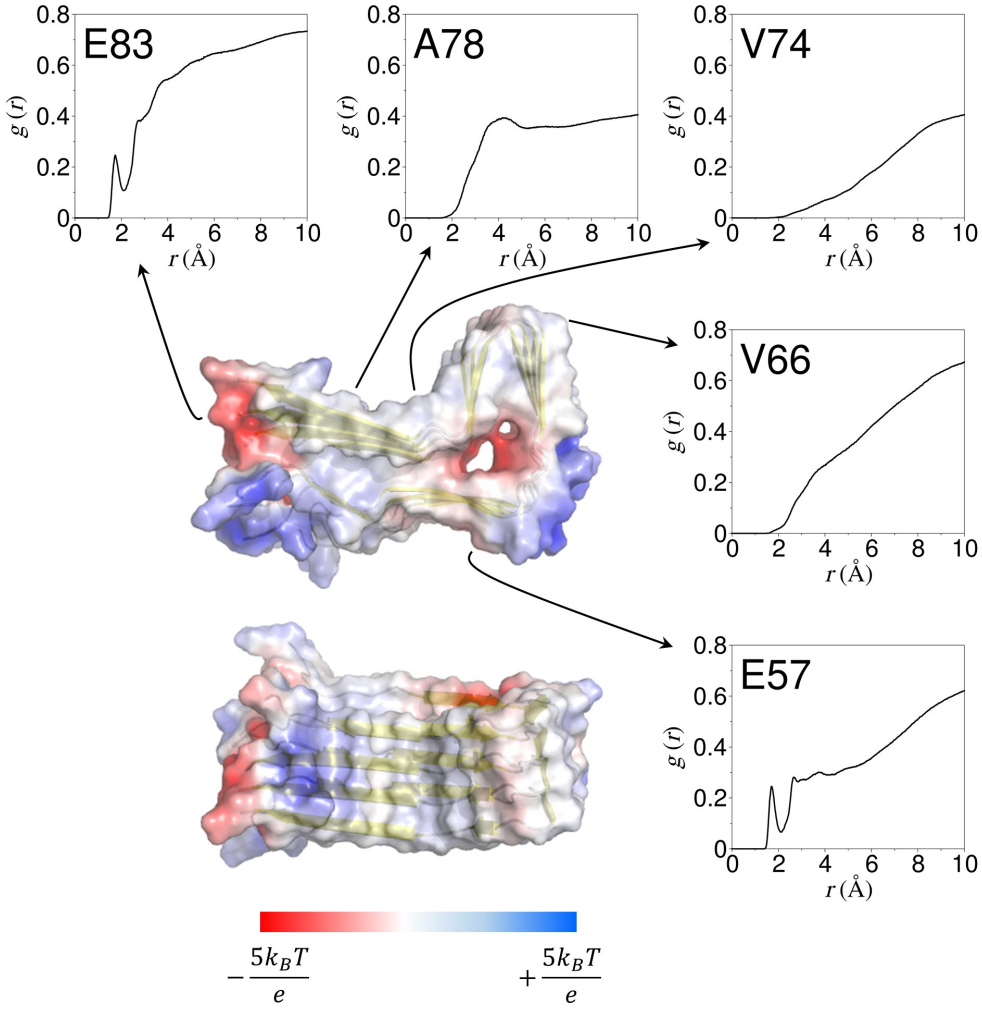

Figure 5.4.5.

Electrostatic potential maps at the solvent accessible surface from the simulation of twister polymorph with a single protofilament, with radial distribution functions of water around A78, V74, V66, E83, and E57.

6. CONCLUSION

In this thesis, we have performed molecular dynamics simulations using the experimentally identified structures of two major fibril polymorphs of wild type α-synuclein and analyzed the structural features and compared the results in detail. From these results, the predominance of rod polymorph in various experimental studies could be explained in terms of its high structural stability in aqueous environments which are obtained by cooperative contributions of various conformational stabilizing features. The rod and twister polymorphs have different interface sequences. The rod polymorph has preNAC ($_{46}$EGVVHGVATVA$_{56}$) interface and the twister polymorph has NACore ($_{68}$GAVVTGVTAVA$_{78}$) interface where both sequences form steric zipper interfaces. The NACore sequence is included in the highly hydrophobic NAC (61-95) region.

It should be noted that all six familial PD mutations (E46K, H50Q, G51D, A53E, A53T, and A53V) are associated with the preNAC sequence. From simple energy calculation analysis, Li et al[35] proposed that all these mutants are likely to disfavor the rod structure. However, it can also be interpreted that the NACore interface is less associated with pathogenicity of α-synuclein fibril. In other words, twister polymorph is not likely to be a major pathogenic strain. Therefore, rather than transforming into twister polymorph, familial PD mutations would induce a slightly different, or

modified rod polymorph structures compared to the rod polymorph structure of wild type α-synuclein, resulting in the change in the composition of polymorphic α-synuclein fibril, which consequently changes pathogenicity. There is an experimental evidence that the familial mutants have similar shape to wild type rod polymorph[54-56]. According to these observations, familial mutations are not expected to induce the transformation into twister structure. Rather, the stable interaction in the preNAC interface disturbed by familial mutations could be recovered by modifying the interface, leading to a new structure which is geometrically not completely different from wild type rod structure. This is a rational expectation because in this way, various favorable structural features of rod polymorph could be largely maintained, compared to the transformation into twister polymorph. Recent high resolution cryo-EM fibril structure of α-synuclein E46K mutant supports this aspect. Eisenberg et al[57] hypothesized that there is a deeper energy state than wild type rod polymorph structure into which the folding pathway is kinetically trapped by E46-K80 salt bridge interaction. The E46K mutation eliminates this trap and unlocks a more stable pathogenic structure. Although this structure is a vast rearrangement from wild type rod structure, it looks more like a rod than twister structure. In fact, the protofilament interface forms at residues 45 to 57 for E46K which is almost identical to preNAC sequence but does not overlap with NACore sequence. In conclusion, we expect that rod polymorph is a major pathogenic strain of wild type α-synuclein fibril. We expect this work could provide a basic

explanation on the pathogenicity of various fibril structures of α-synuclein and other amyloid peptides. In order to achieve overall understanding on the mechanisms of how α-synuclein and other amyloid fibril polymorphisms play a role in derivation of pathogenicity, further experimental and computational research will be needed.

BIBLIOGRAPHY

1. Dickson, D. W., Parkinson's disease and parkinsonism: neuropathology. *Cold Spring Harb Perspect Med* **2012,** *2* (8).

2. Pringsheim, T.; Jette, N.; Frolkis, A.; Steeves, T. D., The prevalence of Parkinson's disease: a systematic review and meta-analysis. *Mov Disord* **2014,** *29* (13), 1583-90.

3. Polymeropoulos, M. H.; Higgins, J. J.; Golbe, L. I.; Johnson, W. G.; Ide, S. E.; Di Iorio, G.; Sanges, G.; Stenroos, E. S.; Pho, L. T.; Schaffer, A. A.; Lazzarini, A. M.; Nussbaum, R. L.; Duvoisin, R. C., Mapping of a gene for Parkinson's disease to chromosome 4q21-q23. *Science* **1996,** *274* (5290), 1197-9.

4. Hornykiewicz, O., The discovery of dopamine deficiency in the parkinsonian brain. *J Neural Transm Suppl* **2006,** (70), 9-15.

5. Katzenschlager, R.; Lees, A. J., Treatment of Parkinson's disease: levodopa as the first choice. *J Neurol* **2002,** *249 Suppl 2*, II19-24.

6. Forno, L. S., Neuropathology of Parkinson's disease. *J Neuropathol Exp Neurol* **1996,** *55* (3), 259-72.

7. Spillantini, M. G.; Schmidt, M. L.; Lee, V. M.; Trojanowski, J. Q.; Jakes, R.; Goedert, M., Alpha-synuclein in Lewy bodies. *Nature* **1997,** *388* (6645), 839-40.

8. Chartier-Harlin, M. C.; Kachergus, J.; Roumier, C.; Mouroux, V.; Douay, X.; Lincoln, S.; Levecque, C.; Larvor, L.; Andrieux, J.; Hulihan, M.; Waucquier, N.; Defebvre, L.; Amouyel, P.; Farrer, M.; Destee, A., Alpha-synuclein locus duplication as a cause of familial Parkinson's disease. *Lancet* **2004,** *364* (9440), 1167-9.

9. Ross, O. A.; Braithwaite, A. T.; Skipper, L. M.; Kachergus, J.; Hulihan, M. M.; Middleton, F. A.; Nishioka, K.; Fuchs, J.; Gasser, T.; Maraganore, D. M.; Adler, C. H.; Larvor, L.; Chartier-Harlin, M. C.; Nilsson, C.; Langston, J. W.; Gwinn, K.; Hattori, N.; Farrer, M. J., Genomic investigation of alpha-synuclein multiplication and parkinsonism. *Ann Neurol* **2008,** *63* (6), 743-50.

10. Conway, K. A.; Harper, J. D.; Lansbury, P. T., Accelerated in vitro

fibril formation by a mutant alpha-synuclein linked to early-onset Parkinson disease. *Nat Med* **1998,** *4* (11), 1318-20.

11. Fortin, D. L.; Troyer, M. D.; Nakamura, K.; Kubo, S.; Anthony, M. D.; Edwards, R. H., Lipid rafts mediate the synaptic localization of alpha-synuclein. *J Neurosci* **2004,** *24* (30), 6715-23.

12. Kahle, P. J.; Neumann, M.; Ozmen, L.; Muller, V.; Jacobsen, H.; Schindzielorz, A.; Okochi, M.; Leimer, U.; van Der Putten, H.; Probst, A.; Kremmer, E.; Kretzschmar, H. A.; Haass, C., Subcellular localization of wild-type and Parkinson's disease-associated mutant alpha -synuclein in human and transgenic mouse brain. *J Neurosci* **2000,** *20* (17), 6365-73.

13. Sawaya, M. R.; Sambashivan, S.; Nelson, R.; Ivanova, M. I.; Sievers, S. A.; Apostol, M. I.; Thompson, M. J.; Balbirnie, M.; Wiltzius, J. J.; McFarlane, H. T.; Madsen, A. O.; Riekel, C.; Eisenberg, D., Atomic structures of amyloid cross-beta spines reveal varied steric zippers. *Nature* **2007,** *447* (7143), 453-7.

14. Maji, S. K.; Wang, L.; Greenwald, J.; Riek, R., Structure-activity relationship of amyloid fibrils. *FEBS Lett* **2009,** *583* (16), 2610-7.

15. Hoyer, W.; Antony, T.; Cherny, D.; Heim, G.; Jovin, T. M.; Subramaniam, V., Dependence of alpha-synuclein aggregate morphology on solution conditions. *J Mol Biol* **2002,** *322* (2), 383-93.

16. Mehra, S.; Sahay, S.; Maji, S. K., alpha-Synuclein misfolding and aggregation: Implications in Parkinson's disease pathogenesis. *Biochim Biophys Acta Proteins Proteom* **2019,** *1867* (10), 890-908.

17. Winner, B.; Jappelli, R.; Maji, S. K.; Desplats, P. A.; Boyer, L.; Aigner, S.; Hetzer, C.; Loher, T.; Vilar, M.; Campioni, S.; Tzitzilonis, C.; Soragni, A.; Jessberger, S.; Mira, H.; Consiglio, A.; Pham, E.; Masliah, E.; Gage, F. H.; Riek, R., In vivo demonstration that alpha-synuclein oligomers are toxic. *Proc Natl Acad Sci U S A* **2011,** *108* (10), 4194-9.

18. Karpinar, D. P.; Balija, M. B.; Kugler, S.; Opazo, F.; Rezaei-Ghaleh, N.; Wender, N.; Kim, H. Y.; Taschenberger, G.; Falkenburger, B. H.; Heise, H.; Kumar, A.; Riedel, D.; Fichtner, L.; Voigt, A.; Braus, G. H.; Giller, K.; Becker, S.; Herzig, A.; Baldus, M.; Jackle, H.; Eimer, S.; Schulz, J. B.; Griesinger, C.; Zweckstetter, M., Pre-fibrillar alpha-synuclein variants with impaired beta-structure increase neurotoxicity in Parkinson's disease models. *EMBO J* **2009,** *28* (20), 3256-68.

19. Volles, M. J.; Lansbury, P. T., Jr., Zeroing in on the pathogenic form of alpha-synuclein and its mechanism of neurotoxicity in Parkinson's

disease. *Biochemistry* **2003,** *42* (26), 7871-8.

20. Goldberg, M. S.; Lansbury, P. T., Jr., Is there a cause-and-effect relationship between alpha-synuclein fibrillization and Parkinson's disease? *Nat Cell Biol* **2000,** *2* (7), E115-9.

21. Cookson, M. R.; Hardy, J.; Lewis, P. A., Genetic neuropathology of Parkinson's disease. *Int J Clin Exp Pathol* **2008,** *1* (3), 217-31.

22. Gaig, C.; Marti, M. J.; Ezquerra, M.; Rey, M. J.; Cardozo, A.; Tolosa, E., G2019S LRRK2 mutation causing Parkinson's disease without Lewy bodies. *J Neurol Neurosurg Psychiatry* **2007,** *78* (6), 626-8.

23. Luk, K. C.; Song, C.; O'Brien, P.; Stieber, A.; Branch, J. R.; Brunden, K. R.; Trojanowski, J. Q.; Lee, V. M., Exogenous alpha-synuclein fibrils seed the formation of Lewy body-like intracellular inclusions in cultured cells. *Proc Natl Acad Sci U S A* **2009,** *106* (47), 20051-6.

24. Luk, K. C.; Kehm, V.; Carroll, J.; Zhang, B.; O'Brien, P.; Trojanowski, J. Q.; Lee, V. M., Pathological alpha-synuclein transmission initiates Parkinson-like neurodegeneration in nontransgenic mice. *Science* **2012,** *338* (6109), 949-53.

25. Volpicelli-Daley, L. A.; Luk, K. C.; Lee, V. M., Addition of exogenous alpha-synuclein preformed fibrils to primary neuronal cultures to seed recruitment of endogenous alpha-synuclein to Lewy body and Lewy neurite-like aggregates. *Nat Protoc* **2014,** *9* (9), 2135-46.

26. Jucker, M.; Walker, L. C., Self-propagation of pathogenic protein aggregates in neurodegenerative diseases. *Nature* **2013,** *501* (7465), 45-51.

27. Brundin, P.; Melki, R.; Kopito, R., Prion-like transmission of protein aggregates in neurodegenerative diseases. *Nat Rev Mol Cell Biol* **2010,** *11* (4), 301-7.

28. Aguzzi, A.; Rajendran, L., The transcellular spread of cytosolic amyloids, prions, and prionoids. *Neuron* **2009,** *64* (6), 783-90.

29. Spillantini, M. G.; Crowther, R. A.; Jakes, R.; Cairns, N. J.; Lantos, P. L.; Goedert, M., Filamentous alpha-synuclein inclusions link multiple system atrophy with Parkinson's disease and dementia with Lewy bodies. *Neurosci Lett* **1998,** *251* (3), 205-8.

30. Spillantini, M. G.; Crowther, R. A.; Jakes, R.; Hasegawa, M.; Goedert, M., alpha-Synuclein in filamentous inclusions of Lewy bodies from Parkinson's disease and dementia with lewy bodies. *Proc Natl Acad*

Sci U S A **1998,** *95* (11), 6469-73.

31. Angot, E.; Steiner, J. A.; Lema Tome, C. M.; Ekstrom, P.; Mattsson, B.; Bjorklund, A.; Brundin, P., Alpha-synuclein cell-to-cell transfer and seeding in grafted dopaminergic neurons in vivo. *PLoS One* **2012,** *7* (6), e39465.

32. Bousset, L.; Pieri, L.; Ruiz-Arlandis, G.; Gath, J.; Jensen, P. H.; Habenstein, B.; Madiona, K.; Olieric, V.; Bockmann, A.; Meier, B. H.; Melki, R., Structural and functional characterization of two alpha-synuclein strains. *Nat Commun* **2013,** *4*, 2575.

33. Peelaerts, W.; Bousset, L.; Van der Perren, A.; Moskalyuk, A.; Pulizzi, R.; Giugliano, M.; Van den Haute, C.; Melki, R.; Baekelandt, V., alpha-Synuclein strains cause distinct synucleinopathies after local and systemic administration. *Nature* **2015,** *522* (7556), 340-4.

34. Peng, C.; Gathagan, R. J.; Covell, D. J.; Medellin, C.; Stieber, A.; Robinson, J. L.; Zhang, B.; Pitkin, R. M.; Olufemi, M. F.; Luk, K. C.; Trojanowski, J. Q.; Lee, V. M., Cellular milieu imparts distinct pathological alpha-synuclein strains in alpha-synucleinopathies. *Nature* **2018,** *557* (7706), 558-563.

35. Li, B.; Ge, P.; Murray, K. A.; Sheth, P.; Zhang, M.; Nair, G.; Sawaya, M. R.; Shin, W. S.; Boyer, D. R.; Ye, S.; Eisenberg, D. S.; Zhou, Z. H.; Jiang, L., Cryo-EM of full-length alpha-synuclein reveals fibril polymorphs with a common structural kernel. *Nat Commun* **2018,** *9* (1), 3609.

36. Guerrero-Ferreira, R.; Taylor, N. M.; Mona, D.; Ringler, P.; Lauer, M. E.; Riek, R.; Britschgi, M.; Stahlberg, H., Cryo-EM structure of alpha-synuclein fibrils. *Elife* **2018,** *7*.

37. Li, Y.; Zhao, C.; Luo, F.; Liu, Z.; Gui, X.; Luo, Z.; Zhang, X.; Li, D.; Liu, C.; Li, X., Amyloid fibril structure of alpha-synuclein determined by cryo-electron microscopy. *Cell Res* **2018,** *28* (9), 897-903.

38. Vilar, M.; Chou, H. T.; Luhrs, T.; Maji, S. K.; Riek-Loher, D.; Verel, R.; Manning, G.; Stahlberg, H.; Riek, R., The fold of alpha-synuclein fibrils. *Proc Natl Acad Sci U S A* **2008,** *105* (25), 8637-42.

39. Der-Sarkissian, A.; Jao, C. C.; Chen, J.; Langen, R., Structural organization of alpha-synuclein fibrils studied by site-directed spin labeling. *J Biol Chem* **2003,** *278* (39), 37530-5.

40. Rodriguez, J. A.; Ivanova, M. I.; Sawaya, M. R.; Cascio, D.; Reyes, F. E.; Shi, D.; Sangwan, S.; Guenther, E. L.; Johnson, L. M.; Zhang, M.;

Jiang, L.; Arbing, M. A.; Nannenga, B. L.; Hattne, J.; Whitelegge, J.; Brewster, A. S.; Messerschmidt, M.; Boutet, S.; Sauter, N. K.; Gonen, T.; Eisenberg, D. S., Structure of the toxic core of alpha-synuclein from invisible crystals. *Nature* **2015,** *525* (7570), 486-90.

41. Tuttle, M. D.; Comellas, G.; Nieuwkoop, A. J.; Covell, D. J.; Berthold, D. A.; Kloepper, K. D.; Courtney, J. M.; Kim, J. K.; Barclay, A. M.; Kendall, A.; Wan, W.; Stubbs, G.; Schwieters, C. D.; Lee, V. M.; George, J. M.; Rienstra, C. M., Solid-state NMR structure of a pathogenic fibril of full-length human alpha-synuclein. *Nat Struct Mol Biol* **2016,** *23* (5), 409-15.

42. Crowther, R. A.; Daniel, S. E.; Goedert, M., Characterisation of isolated alpha-synuclein filaments from substantia nigra of Parkinson's disease brain. *Neurosci Lett* **2000,** *292* (2), 128-30.

43. Jorgensen, W. L.; Chandrasekhar, J.; Madura, J. D.; Impey, R. W.; Klein, M. L., Comparison of simple potential functions for simulating liquid water. *J Chem Phys* **1983,** *79* (2), 926-935.

44. Bjelkmar, P.; Larsson, P.; Cuendet, M. A.; Hess, B.; Lindahl, E., Implementation of the CHARMM force field in GROMACS: Analysis of protein stability effects from correction maps, virtual interaction sites, and water models. *J Chem Theory Comput* **2010,** *6* (2), 459-466.

45. Bussi, G.; Donadio, D.; Parrinello, M., Canonical sampling through velocity rescaling. *J Chem Phys* **2007,** *126* (1), 014101.

46. Berendsen, H. J. C.; Postma, J. P. M.; van Gunsteren, W. F.; Dinola, A.; Haak, J. R., Molecular dynamics with coupling to an external bath. *J Chem Phys* **1984,** *81* (8), 3684-3690.

47. Parrinello, M.; Rahman, A., Polymorphic transitions in single crystals: A new molecular dynamics method *J Appl Phys* **1981,** *52* (12), 7182-7190.

48. Hess, B.; Bekker, H.; Berendsen, H. J. C.; Fraaije, J. G. E. M., LINCS: A linear constraint solver for molecular simulations. *J Comput Chem* **1997,** *18* (12), 1463-1472.

49. Abraham, M. J.; Murtola, T.; Schulz, R.; Páll, S.; Smith, J. C.; Hess, B.; Lindahl, E., GROMACS: High performance molecular simulations through multi-level parallelism from laptops to supercomputers. *SoftwareX* **2015,** *1-2*, 19-25.

50. Touw, W. G.; Baakman, C.; Black, J.; te Beek, T. A. H.; Krieger, E.; Joosten, R. P.; Vriend, G., A series of PDB-related databanks for everyday

needs. *Nucleic Acids Research* **2014,** *43* (D1), D364-D368.

51. Kabsch, W.; Sander, C., Dictionary of protein secondary structure: Pattern recognition of hydrogen-bonded and geometrical features. *Biopolymers* **1983,** *22* (12), 2577-2637.

52. Jurrus, E.; Engel, D.; Star, K.; Monson, K.; Brandi, J.; Felberg, L. E.; Brookes, D. H.; Wilson, L.; Chen, J.; Liles, K.; Chun, M.; Li, P.; Gohara, D. W.; Dolinsky, T.; Konecny, R.; Koes, D. R.; Nielsen, J. E.; Head-Gordon, T.; Geng, W.; Krasny, R.; Wei, G.-W.; Holst, M. J.; McCammon, J. A.; Baker, N. A., Improvements to the APBS biomolecular solvation software suite. *Protein Science* **2018,** *27* (1), 112-128.

53. Schrodinger, LLC, The PyMOL molecular graphics system, version 1.8. 2015.

54. Lemkau, L. R.; Comellas, G.; Kloepper, K. D.; Woods, W. S.; George, J. M.; Rienstra, C. M., Mutant Protein A30P α-Synuclein Adopts Wild-type Fibril Structure, Despite Slower Fibrillation Kinetics*. *Journal of Biological Chemistry* **2012,** *287* (14), 11526-11532.

55. Lemkau, L. R.; Comellas, G.; Lee, S. W.; Rikardsen, L. K.; Woods, W. S.; George, J. M.; Rienstra, C. M., Site-Specific Perturbations of Alpha-Synuclein Fibril Structure by the Parkinson's Disease Associated Mutations A53T and E46K. *PLOS ONE* **2013,** *8* (3), e49750.

56. Comellas, G.; Lemkau, L. R.; Zhou, D. H.; George, J. M.; Rienstra, C. M., Structural Intermediates during α-Synuclein Fibrillogenesis on Phospholipid Vesicles. *Journal of the American Chemical Society* **2012,** *134* (11), 5090-5099.

57. Boyer, D. R.; Li, B.; Sun, C.; Fan, W.; Zhou, K.; Hughes, M. P.; Sawaya, M. R.; Jiang, L.; Eisenberg, D. S., The α-synuclein hereditary mutation E46K unlocks a more stable, pathogenic fibril structure. *Proceedings of the National Academy of Sciences* **2020,** *117* (7), 3592-3602.

국문초록

널리 알려진 신경퇴행성 질병 중 하나인 파킨슨병의 대표적인 병리적 특징은 신경 세포 내의 응집체로 루이 바디라고 불린다. 프리시냅틱 뉴로날 단백질로 알려진 알파시뉴클린의 뭉쳐진 형태가 루이 바디를 구성하는 주요한 구성 물질이라는 점이 밝혀지며 알파시뉴클린에 대한 많은 연구가 진행되고 있다. 최근 ssNMR 그리고 cryo-EM 실험 기법들을 통해 rod 와 twister 라 불리는 두 개의 주요한 알파시뉴클린 피브릴 폴리모프 구조들이 밝혀져 알파시뉴클린의 폴리모피즘을 보였다. 다양한 알파시뉴클린 피브릴 폴리모프가 가지는 다양한 세포독성과 시딩 능력들을 그들의 구조적인 특징으로 연결시켜 이해하기 위해서는 피브릴의 안정성을 구조적인 특징들로 설명하는 것이 필수적이다. 이 논문에서는 두 개의 주요한 와일드타입 알파시뉴클린 피브릴들에 대해 분자 동역학 시뮬레이션을 수행하였다. 물 속 환경에서 피브릴 폴리모프들의 구조 변동과 베타시트 구성을 분석하여 소수성 사이드체인 코어의 패킹, 그를 감싸는 최대 베타시트 구성, 그리고 솔베이션 엔트로피를 최대화하기 위해 큰 구조 변동을 보이는 사이드체인들이라는 특성들이 함께 피브릴

폴리모프들이 물 속 환경에서 안정한 구조를 형성하도록 하였다. 한편, 피브릴 폴리모프 내부에 있는 워터채널과 물에 노출된 표면의 정전기적 포텐셜에너지 분포의 분석을 통해 물과 피브릴과의 직접적인 상호작용이 피브릴 구조의 안정화에 어떻게 기여하는지를 알아보았다. 이 연구를 통해 다양한 아밀로이드 피브릴들이 보이는 여러 병원성의 거동들을 그들이 가지는 여러 구조적인 특징들로 이해할 수 있게 하는 기초가 제공 될 것이라 기대된다.

주요어: 알파시뉴클린, 폴리모피즘, 분자동역학 시뮬레이션, 구조적 안정성, 아밀로이드 피브릴

학 번: 2016-29784